Research Square

Preprints are preliminary reports that have not undergone peer review.
They should not be considered conclusive, used to inform clinical practice,
or referenced by the media as validated information.

Textile-based biosensors for salivary detection of Alzheimer's Disease biomarkers

Bethany Richardson

B.Richardson@derby.ac.uk

University of Derby

Alex Casson

University of Manchester

Christopher Blanford

University of Manchester

Urvashi Gunputh

University of Derby

Research Article

Keywords: Textile biosensors, Alzheimer's Disease, Wearable diagnostics

Posted Date: April 2nd, 2026

DOI: https://doi.org/10.21203/rs.3.rs-9224127/v1

License: This work is licensed under a Creative Commons Attribution 4.0 International License.
Read Full License

Additional Declarations: No competing interests reported.

Abstract

Biosensors convert biochemical reactions into measurable electrical signals and are increasingly used for disease diagnostics. Current Alzheimer's Disease (AD) biomarker detection approaches largely rely on blood or cerebrospinal fluid sampling, which can be invasive and unsuitable for continuous monitoring. This work investigates the feasibility of textile-based biosensors for detecting AD biomarkers in saliva. Interdigitated electrodes were embroidered onto a multilayer textile substrate and coated with graphene oxide (GO), reduced graphene oxide (rGO), AntiTau-GO, and AntiTau-rGO materials. Sensor stability was evaluated through electrical impedance measurements following exposure to water, phosphate buffered saline, artificial saliva, amyloid-β, and Tau proteins. Results indicate that rGO-coated sensors exhibit improved electrical stability compared with GO sensors, while AntiTau-rGO coatings demonstrate enhanced selectivity toward Tau protein.

1. Introduction

Alzheimer's Disease (AD) is a progressive neurodegenerative disorder affecting millions of people worldwide. Early diagnosis remains challenging due to the limited accessibility of diagnostic testing methods. Biomarkers including amyloid-β (Aβ) peptides and Tau proteins are widely used indicators of AD pathology [1]. These biomarkers form the basis of the AT(N) classification framework used in clinical research [2]. Most current biomarker detection approaches rely on blood testing or cerebrospinal fluid analysis, such as 'Lumipulse', received FDA approval in May 2025 which analyses the pTau217/ß-Amyloid 1–42 Plasma Ratio [3]. Although these methods provide reliable diagnostic information, they require invasive sampling and laboratory analysis. Saliva represents an attractive alternative biofluid because it can be collected non-invasively and repeatedly.

Textile-based biosensors are emerging as promising platforms for wearable health monitoring [4]. Conductive threads and nanomaterial coatings can be integrated into fabrics to form flexible sensing systems capable of detecting biochemical signals. Graphene-based materials such as graphene oxide (GO) and reduced graphene oxide (rGO) offer favourable electrical conductivity and surface functionalisation properties for biosensing applications [5].

2. Materials and Methods

2.1 Fabric Substrate

A multilayer textile substrate was used to construct the biosensor. The top layer consisted of cotton fabric for adsorption of graphene ink. A nonwoven gauze layer was used to absorb excess fluid and prevent spreading. A hydrophobic synthetic base layer prevented liquid leakage (Fig. 1.a)

2.2 Embroidered Electrodes

Interdigitated electrodes were embroidered using conductive silver-coated thread on a ZSK embroidery machine. The IDE design consisted of interlocking electrode fingers connected to two contact pads for electrical measurements (Fig. 1.b).

2.3 Graphene Oxide Synthesis

Graphene oxide was synthesised using a modified Hummers method (Fig. 2) [6]. Expandable graphite flakes were oxidised using sulphuric acid and potassium permanganate, followed by washing and centrifugation to obtain GO dispersions.

2.4 Reduction to rGO

Reduced graphene oxide was obtained through chemical reduction of GO using ascorbic acid. The reduction process removed oxygen functional groups and improved electrical conductivity [7].

2.5 AntiTau Functionalisation

AntiTau antibodies were conjugated to graphene surfaces using EDC/NHS chemistry in MES buffer [8]. The functionalised graphene coatings were deposited onto textile electrodes to create selective biosensor surfaces.

2.6 Electrical Measurements

Electrical resistance measurements were performed while droplets of water, phosphate buffered saline, artificial saliva, Aβ and Tau proteins were deposited onto the sensors.

Figure 4. **Schematic of the impedance measurement testing method**

3. Results and Discussion

The performance of the fabricated textile biosensors was evaluated through a combination of microstructural characterisation and electrical sensing experiments. The objective of this section was to determine how the graphene-based coatings influence sensor stability, wettability, and biomarker detection capability.

3.1 Scanning Electron Microscope (SEM)

Scanning Electron Microscope (SEM) imaging confirmed successful coating of graphene materials onto the textile fibres. The SEM images presented (Fig. 5. a – c) confirm that the graphene coatings were successfully deposited onto the embroidered conductive fibres. In the GO-coated sensors (Fig. 5. a), the graphene oxide flakes appear as thin layered structures covering the surface of the silver-coated threads. The flakes exhibit relatively consistent morphology across the sensing region, suggesting that the dropcasting process resulted in a reasonably uniform distribution of the graphene oxide material. The measured flake sizes range approximately between 700 μm and 1500 μm, indicating the presence of

large conductive domains capable of forming electrical pathways across the electrode surface. A higher-magnification image (Fig. 5b) reveals that the graphene flakes adhere closely to the underlying textile fibres while still maintaining the fibrous morphology of the substrate. This is advantageous for textile biosensors, as the porous fibre structure allows interaction with liquid samples while the graphene coating provides electrical conductivity.

In comparison, the rGO-coated sensors (Fig. 5. c) exhibit a slightly more compact surface morphology. This structural difference is consistent with the reduction process, in which oxygen-containing functional groups are removed from the GO structure. The resulting rGO material typically exhibits increased electrical conductivity and a more aggregated graphene network. The denser morphology observed in Fig. 5. c suggests improved electrical contact between graphene domains, which may contribute to the improved electrical stability observed in later experiments.

3.2 Energy-dispersive X-ray spectroscopy (EDS)

Energy-dispersive X-ray spectroscopy was used to determine the elemental composition of the coated sensors and verified the presence of carbon-based graphene structures along with conductive silver threads. The elemental maps presented in Fig. 6 confirm the presence of key elements associated with the biosensor structure. Carbon and oxygen signals dominate the spectra, corresponding to the graphene-based coatings applied to the textile electrodes. The presence of these elements confirms the successful deposition of GO and rGO materials on the sensor surface. Silver signals are also clearly visible in the elemental maps, corresponding to the conductive embroidery thread used to form the interdigitated electrodes.

Minor trace elements, including potassium (0.73%), calcium (2.24%), and manganese (0.5%), were detected in small quantities. These elements are likely residues from the experimental testing phase, particularly from solutions such as phosphate buffered saline. Their presence does not significantly affect sensor operation but indicates that small amounts of test solutions remained on the sensor surface following measurements. Overall, the EDS results confirm that the graphene coatings are present and uniformly distributed across the textile electrodes while maintaining electrical connectivity through the silver thread structure.

3.3 Raman Spectroscopy

Raman spectroscopy was used to confirm the structural characteristics of the graphene materials used in the biosensor coatings. The Raman spectrum shown in Fig. 7 displays two characteristic peaks corresponding to the D band and G band, which are commonly observed in graphene-based materials [9]. The D band, observed at approximately 1351 cm^{-1}, is associated with structural defects or disorder within the graphene lattice. These defects may arise from the oxidation process used during graphene oxide synthesis or from functionalisation of the graphene surface. The presence of a pronounced D peak therefore indicates that the graphene material contains a significant number of defect sites.

The G band appears at approximately 1590 cm^{-1} and corresponds to the in-plane vibration of sp^2 hybridised carbon atoms. This peak is characteristic of graphitic materials and confirms the presence of conductive carbon structures within the coating [10]. The ratio of the D and G band intensities provides insight into the structural quality of the graphene material. In the AntiTau-rGO samples, a slightly higher D-band intensity was observed compared to the plain rGO sensors. This increase is likely due to the introduction of additional surface disorder caused by antibody conjugation. The presence of these functional groups is beneficial for biosensing applications, as defect sites can act as binding locations for biomolecules.

3.4 Contact angle analysis and surface wettability

The wettability of the sensor surfaces was evaluated using contact angle measurements, as shown in Fig. 8. Surface wettability plays an important role in biosensor performance because it influences how liquid samples interact with the sensing region. The plain textile substrate exhibits contact angles greater than 90°, indicating relatively hydrophobic behaviour. This is typical of untreated textile fibres, where water droplets remain on the surface rather than being rapidly absorbed.

In contrast, the GO-coated sensors demonstrate significantly increased hydrophilicity. The water droplets placed on these surfaces were rapidly absorbed into the textile substrate, indicating strong interaction between the graphene oxide coating and the liquid sample. While this hydrophilic behaviour promotes rapid sample spreading, it also introduces variability in electrical measurements because the liquid spreads unpredictably across the sensor surface. The rGO-coated sensors exhibit a more hydrophobic surface compared with GO coatings. The reduction of oxygencontaining functional groups decreases the surface energy of the graphene layer, resulting in slower liquid absorption. This behaviour allows droplets to remain more localized on the sensing region, improving measurement stability and reproducibility.

3.5 Electrical response of GO-coated sensors

The electrical behaviour of the GO-coated sensors is shown in Fig. 9. When droplets of water, phosphate buffered saline, artificial saliva, or Aβ protein are deposited onto the sensor surface at approximately 60 seconds, a significant drop in resistance is observed. This drop in resistance occurs because the added liquid creates a conductive pathway between the electrode fingers of the interdigitated structure. As the liquid spreads across the graphene-coated region, it effectively reduces the electrical resistance measured between the electrodes. However, a notable feature of the GO sensor results is the high variability between repeated experimental runs. The magnitude of resistance change varies by nearly an order of magnitude in some cases. This variability can be attributed to the strong hydrophilic nature of the GO surface, which allows the liquid droplet to spread rapidly and unevenly across the textile substrate. As a result, the GO-coated sensors are highly sensitive to the presence of liquids but lack sufficient stability for reliable biomarker detection.

3.6 Electrical response of rGO-coated sensors

The electrical behaviour of the rGO-coated sensors is presented in Fig. 10. Compared with the GO sensors, the rGO-coated devices exhibit significantly smaller fluctuations in resistance when exposed to the same test solutions. This improved stability can be attributed to several factors. First, the reduction of oxygen functional groups in rGO decreases the hydrophilicity of the graphene surface, resulting in slower liquid absorption. Second, the increased electrical conductivity of rGO provides a more stable baseline resistance. Although rGO sensors demonstrate improved stability, the resistance changes observed following exposure to Aβ are relatively small and inconsistent. This indicates that rGO alone does not provide sufficient selectivity for detecting specific biomarker proteins.

Fig 11 shows comparison in magnitude of the GO-coated and rGO-coated samples.

Figure 11. **Resistance measurement comparisons of GO Sample 1 and GO Sample 2 with added droplets of water, phosphate buffered saline, Artificial Saliva, Aβ**

3.7 AntiTau-GO Samples A and AntiTau-rGO Sample B

Figure 12 investigates the stability of AntiTau-GO Sample A and AntiTau-rGO Sample B

with water, artificial saliva, Aβ and Tau added added to the surfaces across different runs. At time t = 0 s, all test runs show an initial resistance of 10^7 to 10^8 Ω. This is consistent with a dry sensor, or a sensor without a conductive medium present, as is expected for GO-coated sensors in baseline conditions. At approximately 60 seconds, there is a sharp and substantial drop in resistance in all tests, which validates that water was added to the sensor surface at that point. This drop in resistance reflects the sensor's response to the conductive nature of the water, which lowers the resistance by creating a conductive path on the GO-coated surface. The 5 test runs remain at a lower resistance compared to the start of the test, between 10^4 and 10^6 Ω.

Secondly, the stability of AntiTau-GO Sample A when artificial saliva was added to the surface is investigated. At 60 seconds a 0.1 mL droplet of artificial saliva is added to the surface at which point all 5 runs show a sharp decrease in resistance. The remaining time of all 5 test runs shows the resistance stays between 10^4 Ω to 10^5 Ω. Thirdly, when 0.1 mL of Tau protein is dropped onto the surface at time t = 0 seconds, all 5 test runs start at a high resistance value in similar behaviour to the previous graphs. At 60 seconds, when the 0.1 mL of Tau protein is added to the surface, all 5 test runs show a sharp decrease in the resistance, but to different levels of magnitude. The decrease in resistance in this instance ranges between 10^4 and 10^7 Ω suggesting a more complex interaction between Tau and the GO-coated surface.

Finally, the resistance results of the AntiTau-GO Sample A when Aβ protein is added to the surface as a 0.1 mL droplet are displayed. This test was to compare the results of the sensor with a different, non-target, biomarker protein for AD. The starting resistance, at time t = 0 seconds, is between 106 and 108 Ω, consistent with the previous tests. When 0.1 mL of Aβ protein is added, at 60 seconds, there is a comparatively small drop in the resistance of the sample across all 5 test runs. The results in this

experiment show more fluctuations over time compared to when water, artificial saliva, and Tau were added to the sensor surface. This could be due to the Aβ protein aggregating on the sensor surface, or its binding sites interacting differently to the Tau protein, as Aβ is not the target molecule for AntiTau antibody. Therefore the AntiTau coating displays some response to the Aβ protein but a much less stable result when compared with the target protein Tau. AntiTau-functionalised sensors showed improved selectivity for Tau protein compared with amyloid-β, suggesting successful biomolecular recognition.

4. Conclusion

This study demonstrated the feasibility of graphene-based textile biosensors for detecting Alzheimer's Disease biomarkers in saliva. rGO coatings improved electrical stability while AntiTau functionalisation enhanced selectivity for Tau protein. his study demonstrates that the performance of textile-based biosensors is governed by the interplay between graphene material properties and biochemical functionalisation. While GO-coated sensors exhibit high sensitivity, their strong hydrophilicity leads to significant signal variability and poor reproducibility. In contrast, rGO coatings provide enhanced electrical stability and more consistent resistance responses due to improved conductivity and controlled wettability.

The incorporation of AntiTau antibodies enables selective detection of Tau protein, with clear differentiation from amyloid-β responses. Among all configurations, the AntiTaurGO sensors deliver the best overall performance, achieving a balance of stability, sensitivity, and selectivity. These findings highlight the importance of combining optimised nanomaterials with targeted biofunctionalisation for reliable biosensing. Furthermore, the reproducible resistance–time signatures obtained from AntiTau-rGO sensors provide a strong foundation for integration with machine learning algorithms, supporting the development of wearable, non-invasive diagnostic systems for early Alzheimer's disease detection.

Declarations

Author Contribution

B.R completed the project conceptualisation, data collection, data analysis and writing the manuscript. A.C supervised the project, wrote the code for data analysis and reviewed and edited the article. C.B assisted with supervision of the project, wrote code for the Raman Spectrometry imaging analysis. U.G completed the editing of the article.

Acknowledgements

Thank you to Professor Alex Casson and Dr Christopher Blanford at the University of Manchester for their Supervision during this study. Prof. Casson assisted with project conceptualization, data analysis using Python and editing. Dr Blanford assisted with SEM, EDX imaging analysis.

References

1. C. R. Jack *et al.*, A/T/N: An unbiased descriptive classification scheme for Alzheimer disease biomarkers, *Neurology*, vol. 87, no. 5, pp. 539–547, Aug. 2016, doi: 10.1212/WNL.0000000000002923.
2. X. Zeng *et al.*, Alzheimer blood biomarkers: practical guidelines for study design, sample collection, processing, biobanking, measurement and result reporting, *Mol Neurodegeneration*, vol. 19, no. 1, p. 40, May 2024, doi: 10.1186/s13024-02400711-1.
3. FDA Clears First Blood Test for Early Detection of Alzheimer-Linked Amyloid Plaques, AJMC. Accessed: May 22, 2025. [Online]. Available: https://www.ajmc.com/view/fda-clears-first-blood-test-for-early-detection-ofalzheimer-linked-amyloid-plaques
4. J. Kim, A. S. Campbell, B. E.-F. de Ávila, and J. Wang, Wearable biosensors for healthcare monitoring, *Nat Biotechnol*, vol. 37, no. 4, pp. 389–406, Apr. 2019, doi: 10.1038/s41587-019-0045-y.
5. S. M. A. Iqbal, I. Mahgoub, E. Du, M. A. Leavitt, and W. Asghar, Advances in healthcare wearable devices, *npj Flex Electron*, vol. 5, no. 1, p. 9, Apr. 2021, doi: 10.1038/s41528-021-00107-x.
6. G. Nagy, E. Olveti, M. Zeher, S. Márton, and G. Keszthelyi, Use of hydroxy-propylmethyl cellulose (methocel) and carboxy-methyl cellulose containing artificial saliva in the symptomatic treatment of xerostomia, *Fogorv Sz*, vol. 88, no. 9, pp. 299–304, Sep. 1995.
7. T. Chudziak *et al.*, A comparative investigation of the chemical reduction of graphene oxide for electrical engineering applications, *Nanoscale*, vol. 15, no. 44, pp. 17765–17775, 2023, doi: 10.1039/D3NR04521H.
8. B. Pegu, S. Devi, D. J. Sonowal, R. Boruah, and S. Konwer, A comparative study on the synthesis of highly conductive reduced graphene oxide from GO using various green reductant for methanol sensors, *J Mater Sci: Mater Electron*, vol. 35, no. 19, p. 1340, Jul. 2024, doi: 10.1007/s10854-024-13055-9.
9. K. N. Kudin, B. Ozbas, H. C. Schniepp, R. K. Prud'homme, I. A. Aksay, and R. Car, Raman Spectra of Graphite Oxide and Functionalized Graphene Sheets, *Nano Lett.*, vol. 8, no. 1, pp. 36–41, Jan. 2008, doi: 10.1021/nl071822y.
10. R. Muzyka, S. Drewniak, T. Pustelny, M. Chrubasik, and G. Gryglewicz, Characterization of Graphite Oxide and Reduced Graphene Oxide Obtained from Different Graphite Precursors and Oxidized by Different Methods Using Raman Spectroscopy, *Materials*, vol. 11, no. 7, p. 1050, Jun. 2018, doi: 10.3390/ma11071050.

Figures

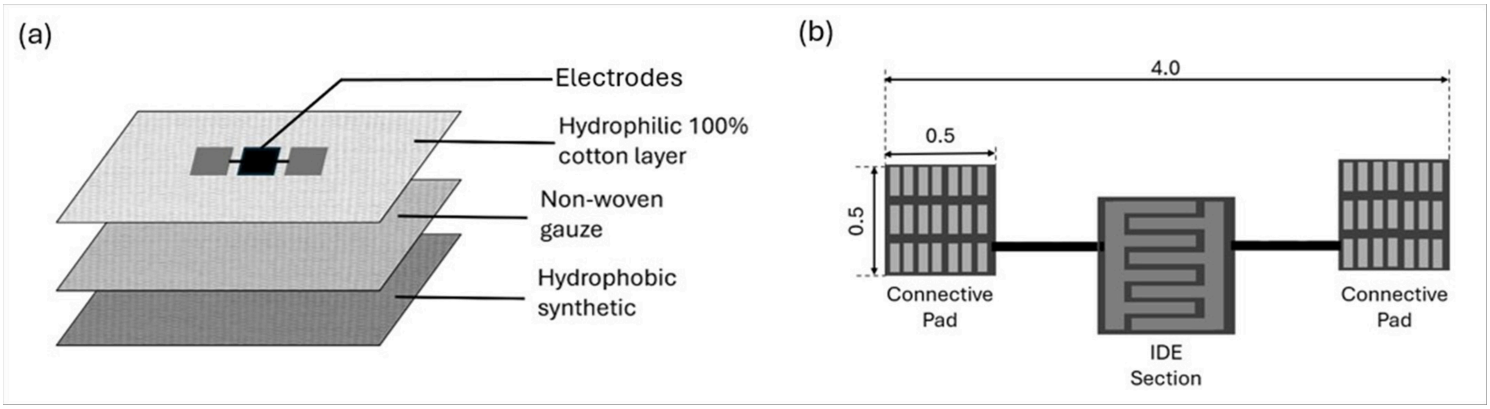


Figure 1

a) Fabric layers with embroidery on surface b) Technical IDE design of embroidered sensor dimension

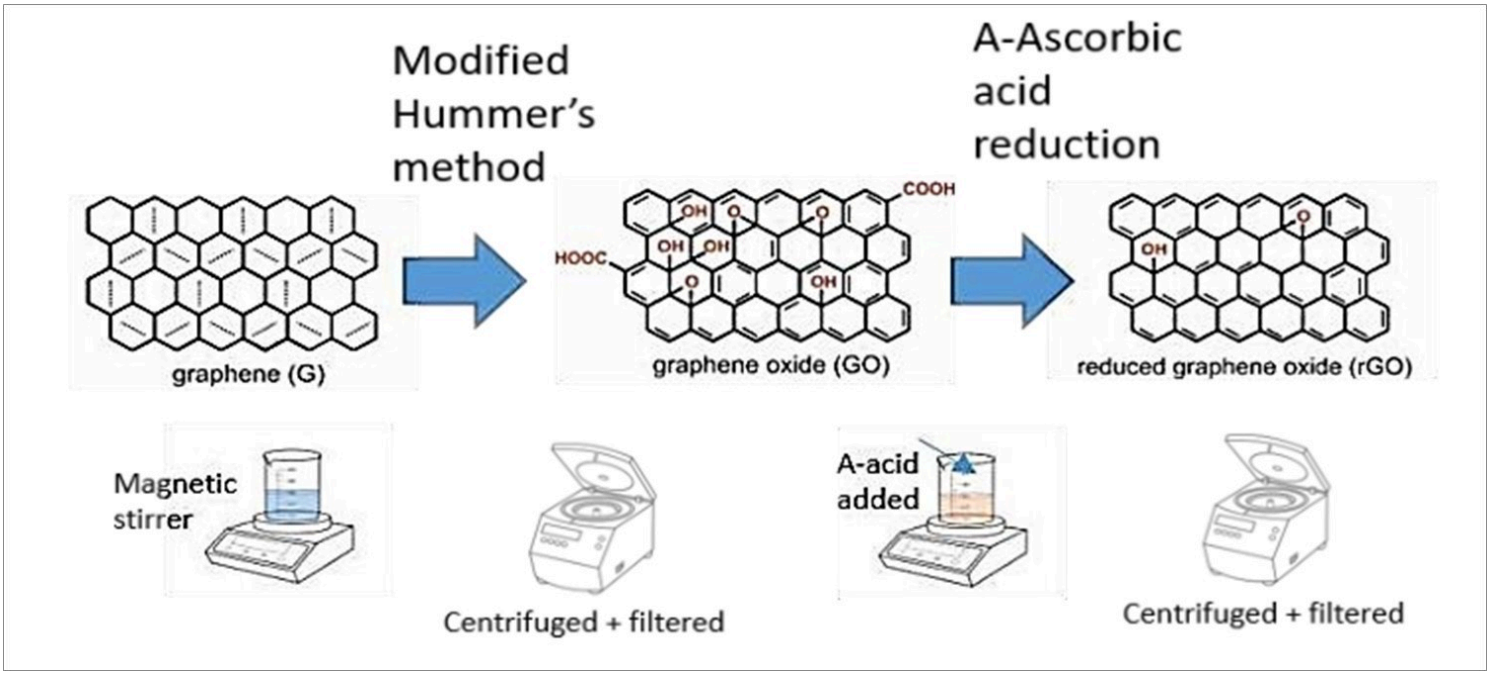


Figure 2

Process of rGO synthesis using A-Ascorbic Acid dispersion in GO ink

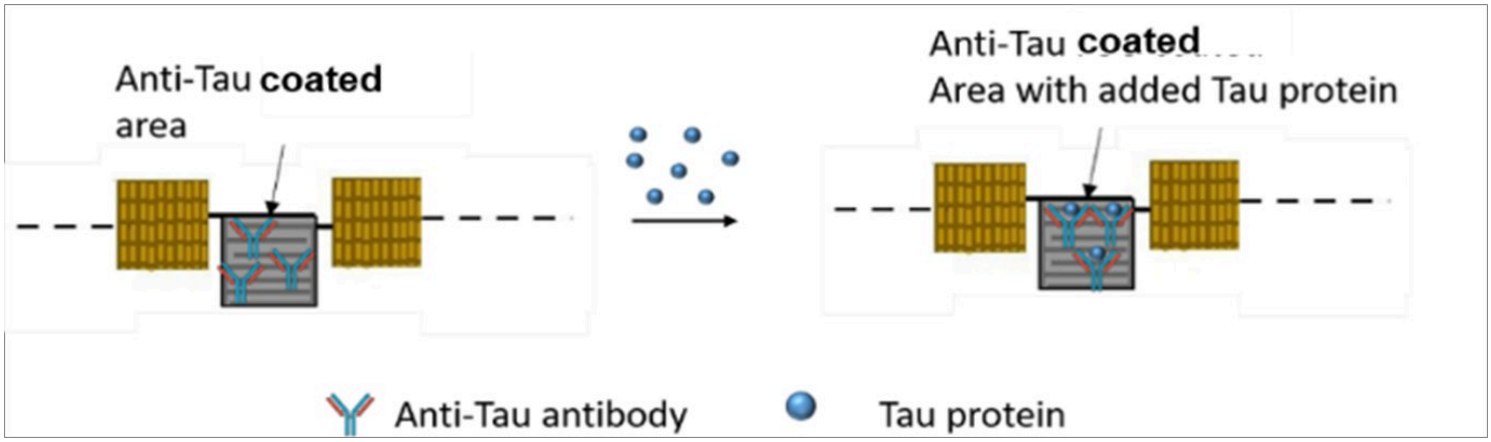


Figure 3

Schematic of the experiment method utilizing antibody-coated sensors

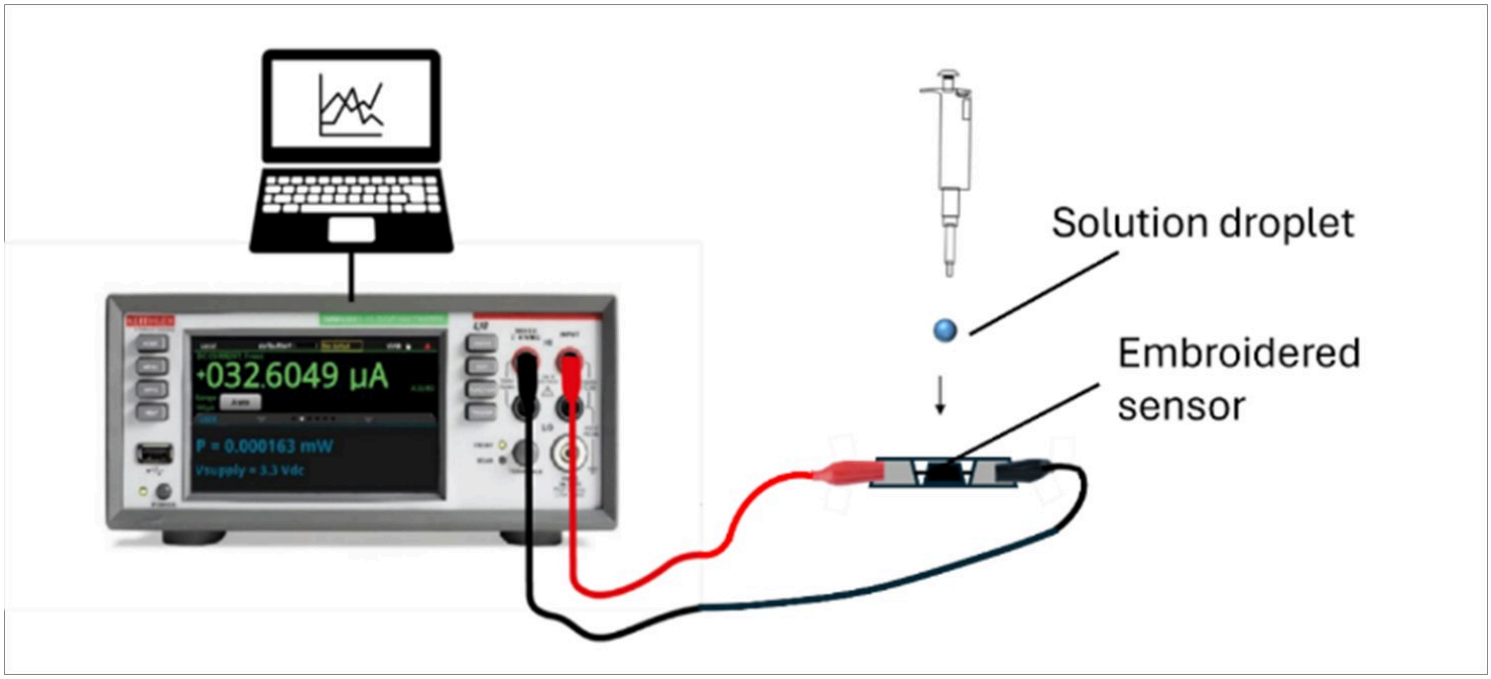


Figure 4

Schematic of the impedance measurement testing method

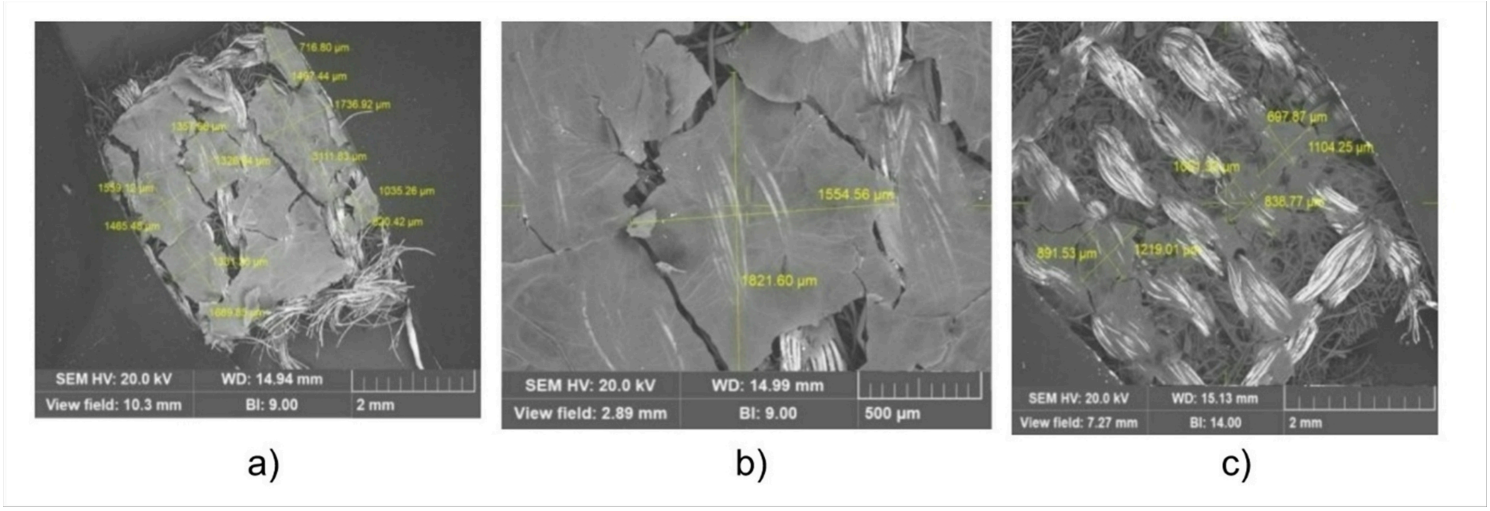


Figure 5

Figure 2. a) SEM image of GO-coated sensor with graphite flake measurements b) SEM image of GO-coated sample c) SEM image of rGO-coated sensor with graphite flake measurements

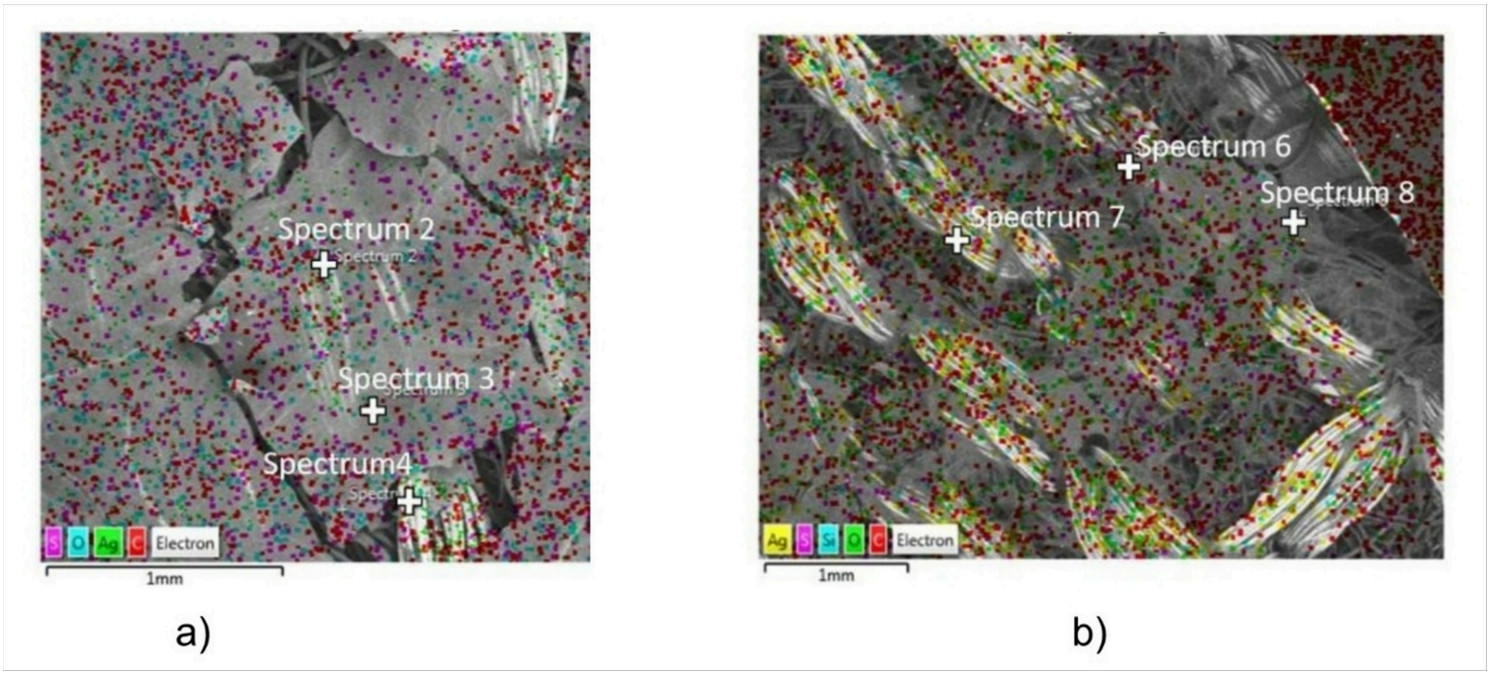


Figure 6

Fig 3. a) EDS image of GO sensor with three spectrums highlighted b) EDS image of rGO sensor with three spectrums highlighted

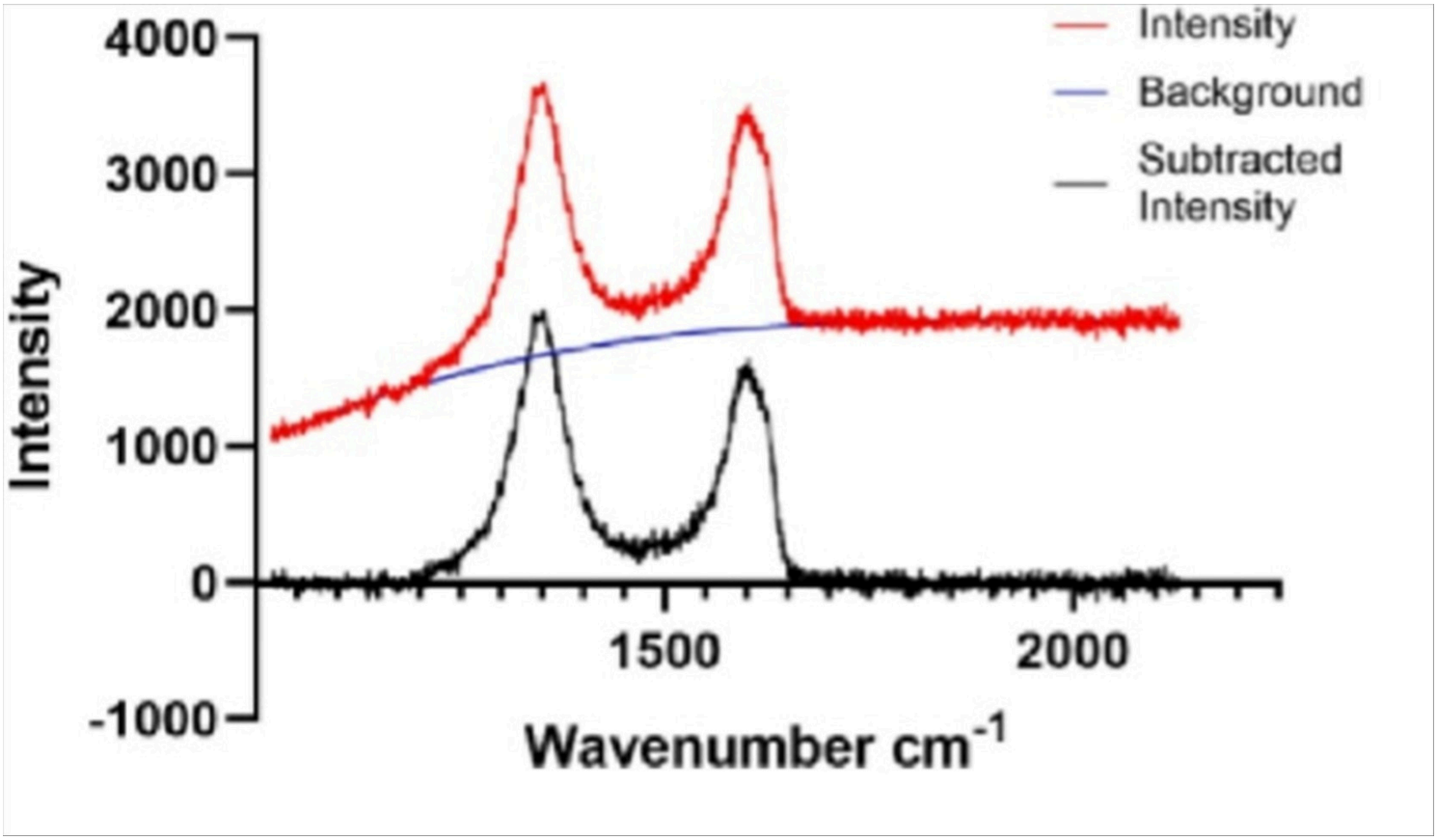


Figure 7

Fig 4. Raman spectrum maps of rGO sample

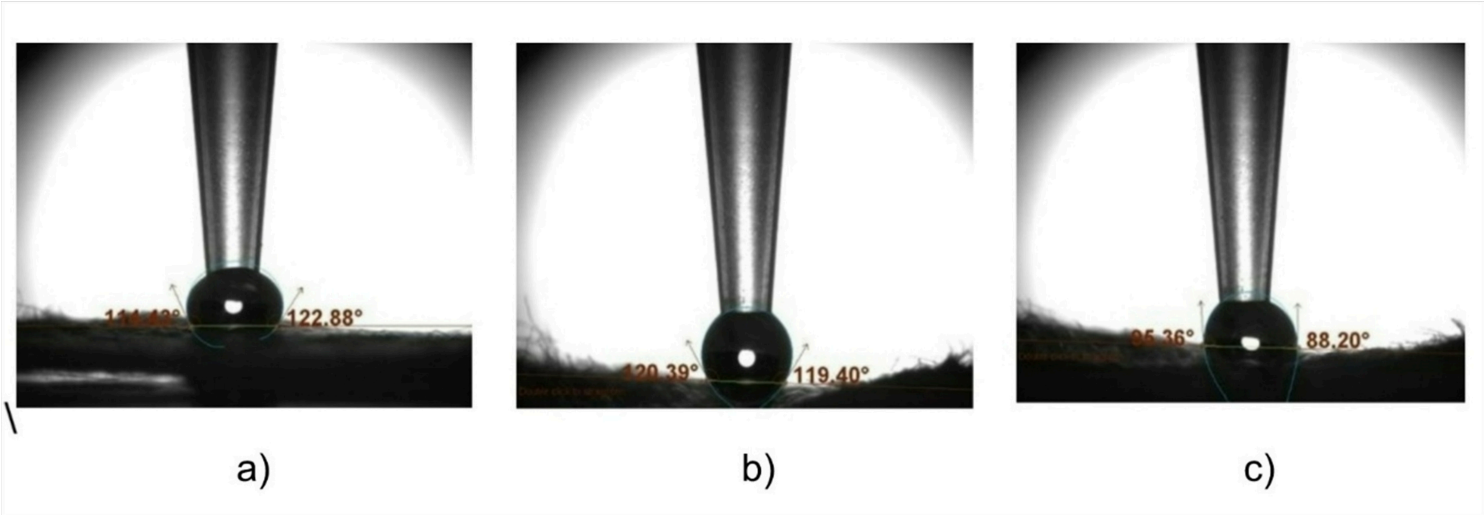


Figure 8

Fig 8. a) Contact angle sessile drop on plain substrate with no coating no embroidery b) Contact angle sessile drop on GO coated substrate c) Contact angle sessile drop on rGO coated substrate

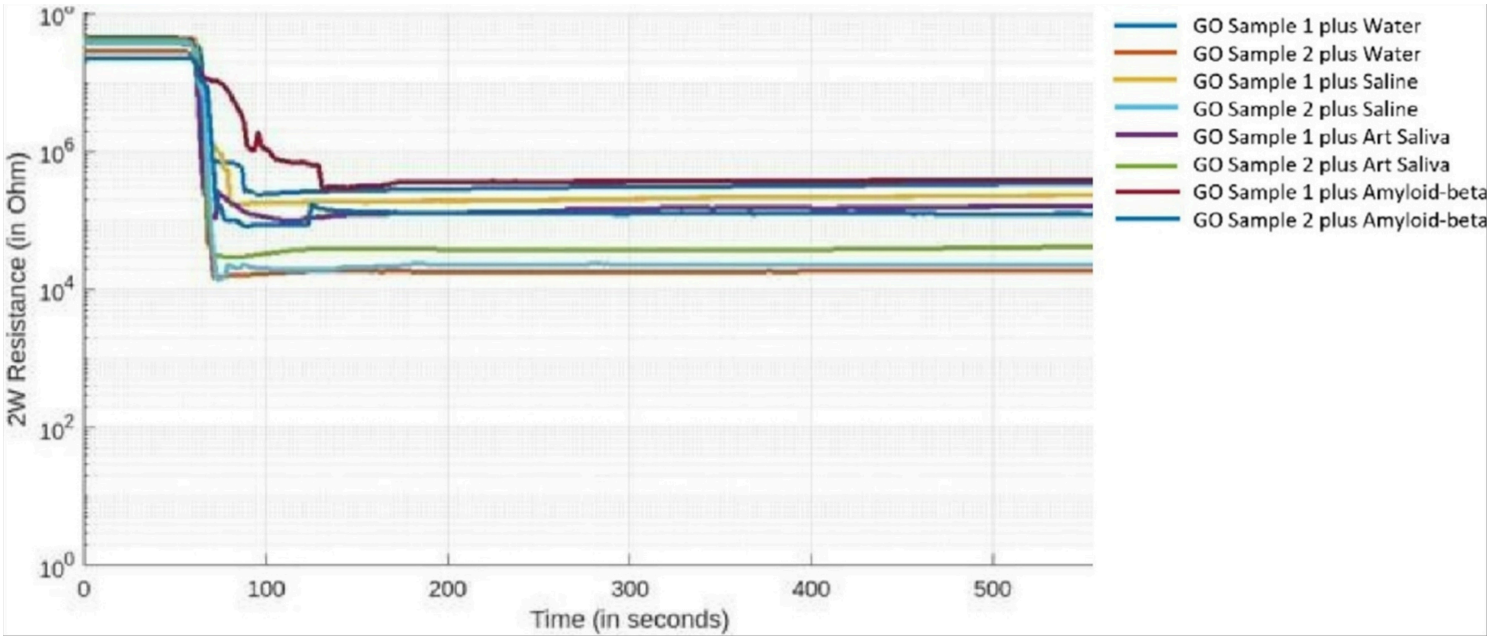


Figure 9

Fig 9. Resistance measurement of GO Sensor Samples 1 and 2 with added droplets of water, Phosphate Buffered Saline, Artificial Saliva and Aβ

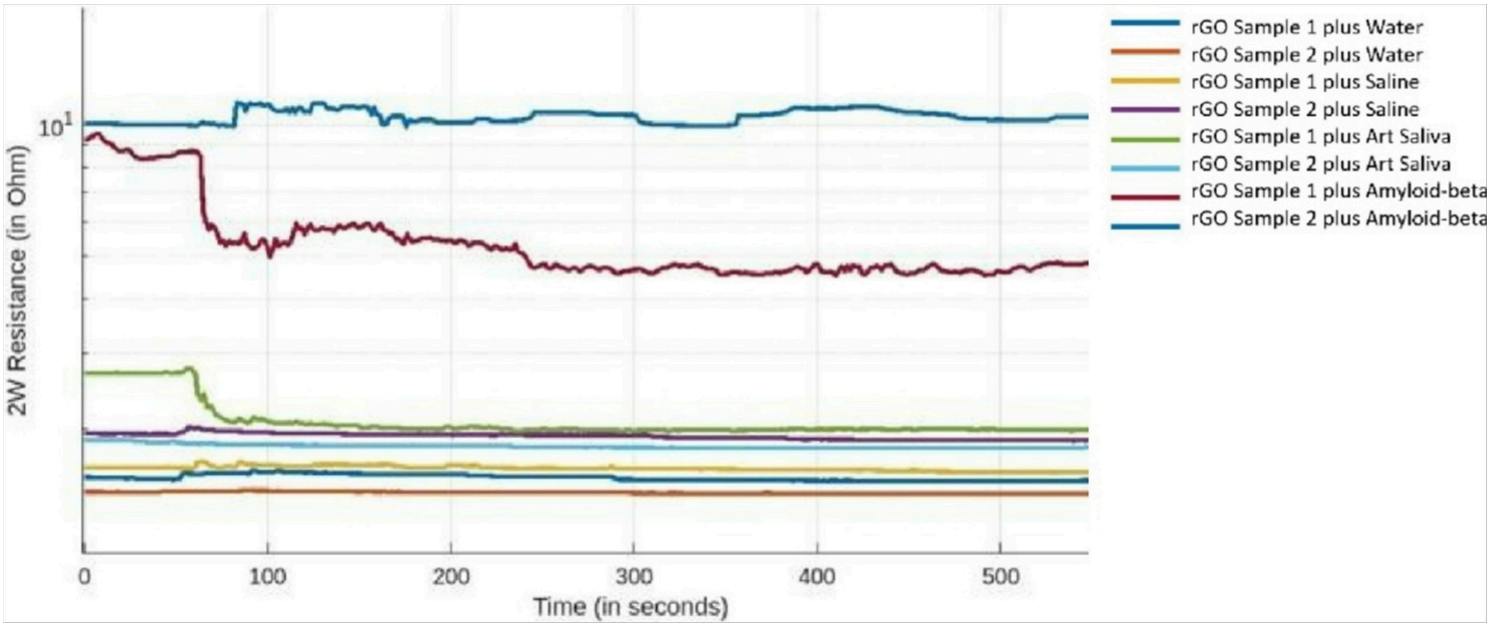


Figure 10

Fig 10. Resistance measurement of rGO Sensor Samples 1 and 2 with added droplets of water, Phosphate Buffered Saline, Artificial Saliva and Aβ

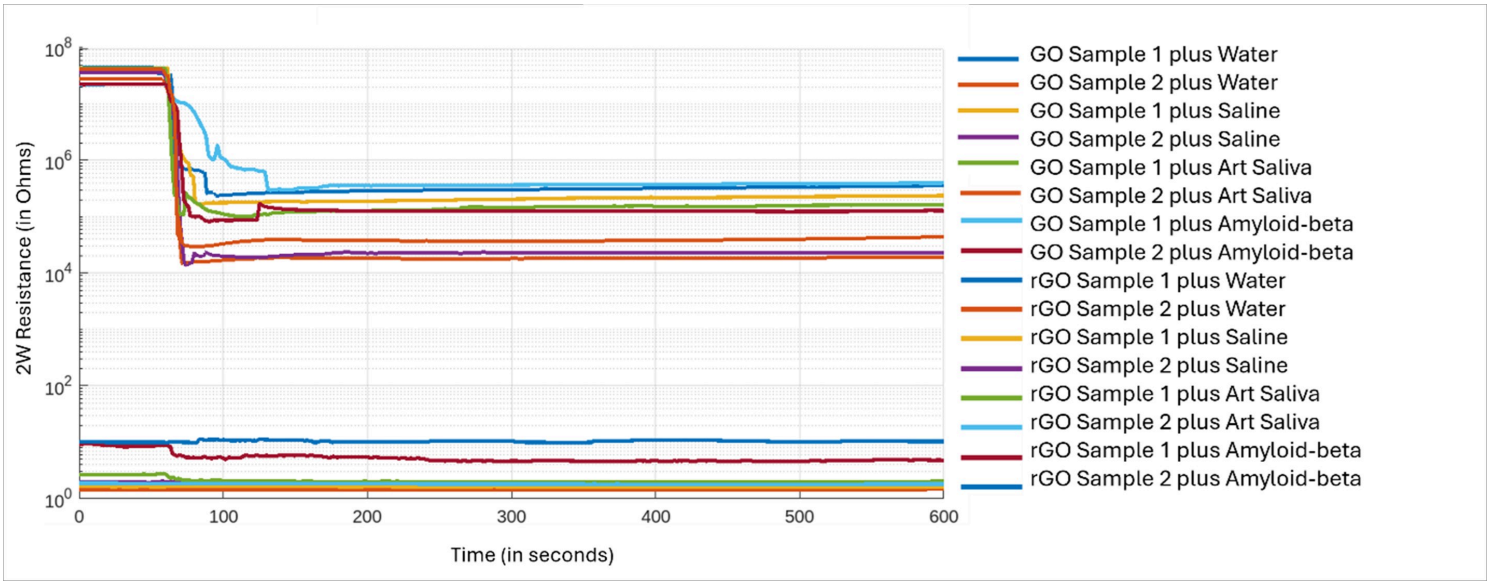


Figure 11

Fig 11. Resistance measurement comparisons of GO Sample 1 and GO Sample 2 with added droplets of water, phosphate buffered saline, Artificial Saliva, Aβ

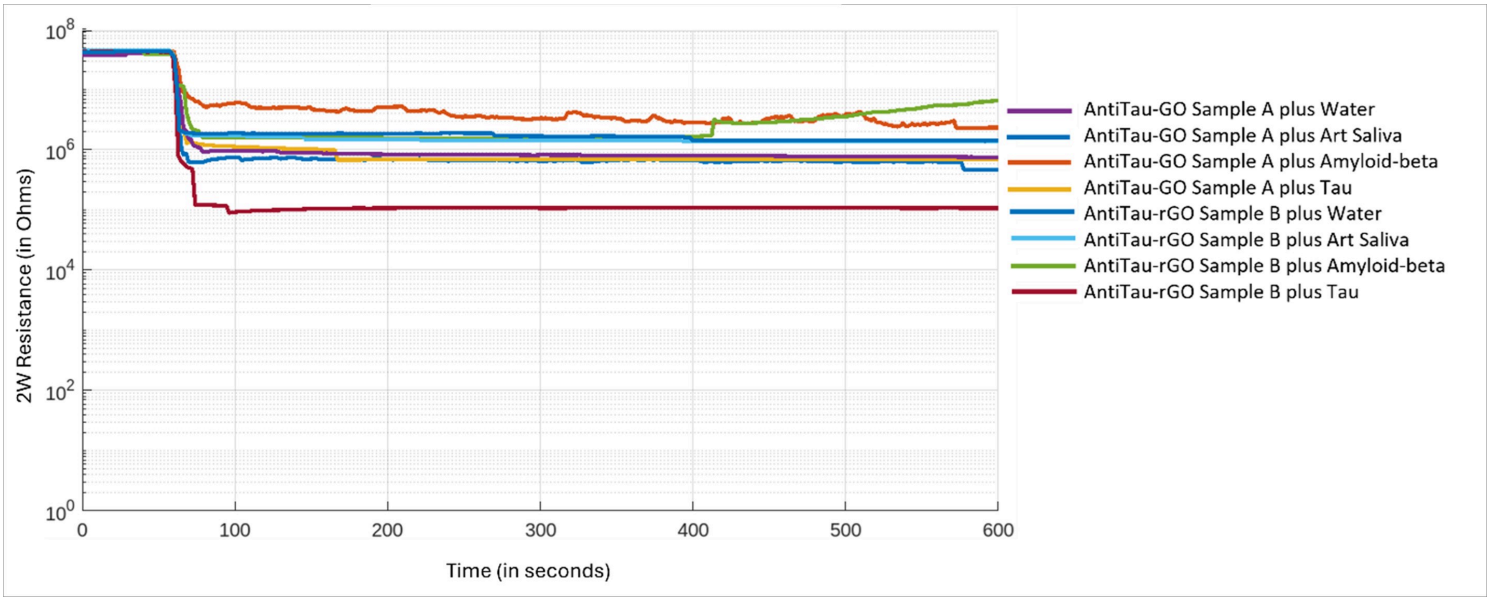


Figure 12

Fig 5. Resistance measurement of AntiTau- GO Sample A and AntiTau-rGO Sample B with added droplets of water, Artificial Saliva, Aβ and Tau

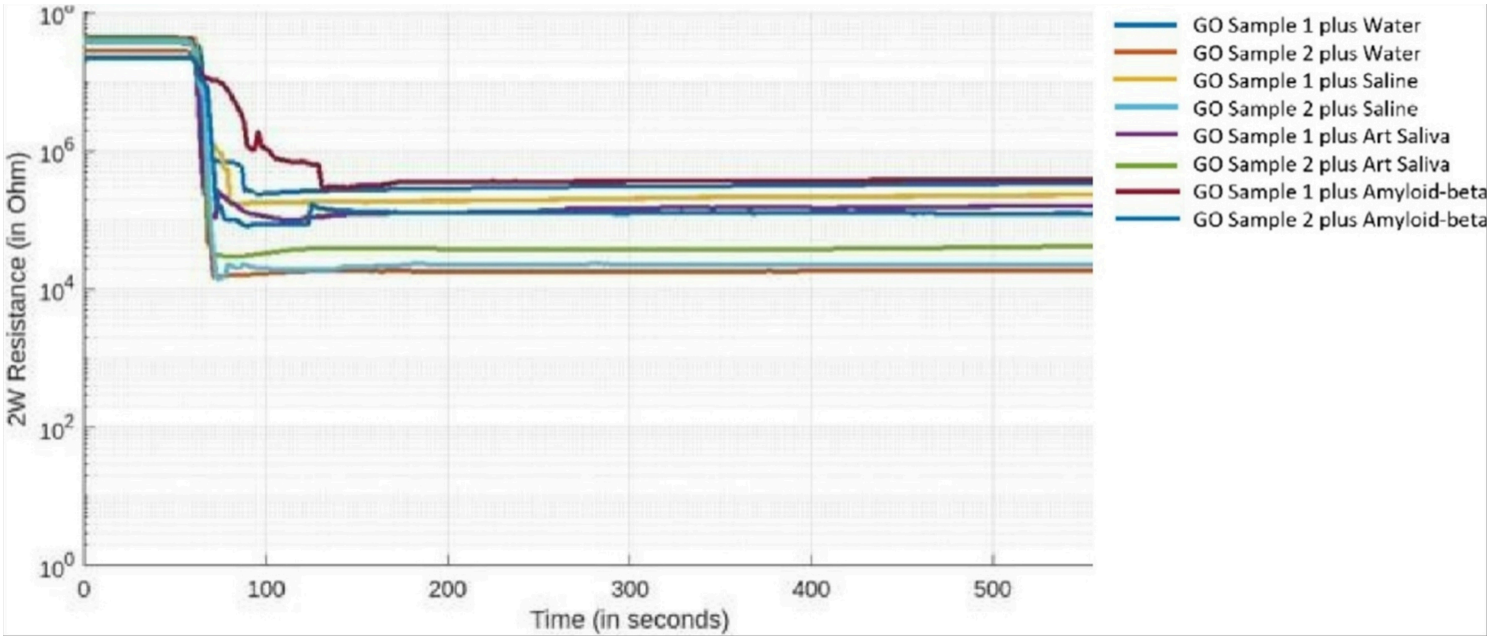


Figure 13

Fig 13. Resistance measurement of GO Sensor Samples 1 and 2 with added droplets of water, Phosphate Buffered Saline, Artificial Saliva and Aβ